NASA TECHNICAL MEMORANDUM

NASA TM X-2610

NASA TM X-2610

A SEARCH FOR THE EFFECT OF A HIGH-FREQUENCY SPARK ON BOUNDARY-LAYER TRANSITION AT MACH 8.5

by John B. Anders, William B. Boatright, and John R. Nayadley, Sr.

Langley Research Center
Hampton, Va. 23365

NATIONAL AERONAUTICS AND SPACE ADMINISTRATION • WASHINGTON, D. C. • AUGUST 1972

1. Report No.	2. Government Accession No.	3. Recipient's Catalog No.
NASA TM X-2610		

4. Title and Subtitle	5. Report Date
A SEARCH FOR THE EFFECT OF A HIGH-FREQUENCY SPARK ON BOUNDARY-LAYER TRANSITION AT MACH 8.5	August 1972
	6. Performing Organization Code

7. Author(s)	8. Performing Organization Report No.
John B. Anders, William B. Boatright, and John R. Nayadley, Sr.	L-8314
	10. Work Unit No. 136-13-01-12
9. Performing Organization Name and Address	11. Contract or Grant No.
NASA Langley Research Center Hampton, Va. 23365	
	13. Type of Report and Period Covered
12. Sponsoring Agency Name and Address	Technical Memorandum
National Aeronautics and Space Administration Washington, D.C. 20546	14. Sponsoring Agency Code

15. Supplementary Notes

16. Abstract

An experimental investigation of the use of a high-frequency spark to promote early boundary-layer transition on a wind-tunnel model was conducted at a Mach number of 8.5. Test variables included four electrode configurations, a frequency range from 10 kHz to 50 kHz, and various power inputs to the spark. The general conclusion obtained from this investigation is that over the parameter range, the high-frequency spark is ineffective in inducing early transition at the test Mach Number.

17. Key Words (Suggested by Author(s))	18. Distribution Statement
Boundary-layer transition High-frequency spark	Unclassified – Unlimited

19. Security Classif. (of this report)	20. Security Classif. (of this page)	21. No. of Pages	22. Price*
Unclassified	Unclassified	24	$3.00

*For sale by the National Technical Information Service, Springfield, Virginia 22151

A SEARCH FOR THE EFFECT OF A HIGH-FREQUENCY SPARK ON BOUNDARY-LAYER TRANSITION AT MACH 8.5

By John B. Anders, William B. Boatright,
and John R. Nayadley, Sr.
Langley Research Center

SUMMARY

An experimental investigation of the use of a high-frequency spark to promote early boundary-layer transition on a wind-tunnel model was conducted at a Mach number of 8.5. Test variables included four electrode configurations, a frequency range from 10 kHz to 50 kHz, and various power inputs to the spark. The general conclusion obtained from this investigation is that over the parameter range, the high-frequency spark is ineffective in inducing early transition at the test Mach number.

INTRODUCTION

Tripping of the laminar boundary layer to generate a turbulent boundary layer at some forward location on a model has proved to be a valuable wind-tunnel test technique at subsonic and supersonic speeds. Various types of roughness strips have been applied and with a relatively small increase in form drag, the roughness strips cause the boundary layer to become turbulent over a major portion of the small wind-tunnel model. The boundary-layer conditions of a large flight vehicle at a high Reynolds number are thus simulated with a small model. As the Mach number increases into the hypersonic speed range, however, artificially induced transition becomes more difficult to apply because the roughness size required for effective tripping increases. This subject has been investigated extensively and references 1 to 5 give guidelines for the sizing, spacing, and drag of roughness trips. Typically, roughness elements in hypersonic flow are 1.5 to 3 times the boundary-layer thickness with some tendency for more effective shapes of the roughness elements to be those with their maximum area concentrated near the top of the trip. Drag of the roughness elements is therefore appreciable (ref. 5). Small discrete jets have also been used to trip hypersonic boundary layers (refs. 6 to 9) and their use appears promising. The turbulent flow downstream of transition induced by the jet trip shows less distortion compared with that downstream of natural transition than the flow downstream of a spherical roughness trip producing the same transition position. However, the normal force created by the jet can be a disadvantage and wind-tunnel-model complexity increases.

Other techniques for moving the transition point include oscillation of a flexible surface skin to delay transition (ref. 10), acoustic excitation to promote transition (ref. 11), and a corona discharge technique (ref. 12). These techniques were investigated at subsonic velocities.

The present experimental investigation represents a cursory look at the possibility of using high-frequency spark pulses to induce early transition. Initial considerations indicate that high-frequency pulses might provide an effective trip with little effect on the form drag of the model. Each spark produces an energy pulse in the flow which creates an impulsive disturbance, and there is the possibility of a periodic disturbance such as a succession of sparks exciting a natural disturbance frequency in the boundary layer with a resonance mechanism. Klein's recent publication (ref. 13), which appeared subsequent to the testing phase of the present investigation, indicates that high-frequency sparks can promote early transition in the Mach number 2 to 4 range. In view of the decreased susceptibility of the laminar boundary layer to conventional roughness-induced disturbances at high Mach numbers, the present experiments at the relatively high Mach number of 8.5 should represent a more severe test of high-frequency-spark transition fixing.

SYMBOLS

c_p	specific heat
f	frequency
M	Mach number
N_{Re}	Reynolds number per meter, $\frac{\rho_\infty V_\infty}{\mu_\infty}$
$N_{Re,x}$	Reynolds number, $\frac{\rho_\infty V_\infty x}{\mu_\infty}$
N_{St}	Stanton number, $\frac{\dot{q}}{\rho_\infty V_\infty c_p (T_{aw} - T_w)}$
$\dot{q}$	heat-transfer rate
T	temperature
t	time

V	velocity
x	distance along plate in stream direction
α	wave number as used in stability theory, ω/V_∞
δ	boundary-layer thickness
ρ	density
τ_s	skin thickness
μ	viscosity
ω	circular frequency, rad/sec

Subscripts:

aw	adiabatic wall
s	steel
w	wall
∞	free stream

APPARATUS AND TESTS

Tunnel

Tests were conducted in the Langley 20-inch hypersonic tunnel (M = 8.5). This is a blowdown wind tunnel with an axisymmetric nozzle exhausting either to a vacuum sphere or to the atmosphere by using an annular ejector. Stagnation temperature for all tests was approximately 810 K and the unit Reynolds number range was from 11.6×10^6 to 17.4×10^6 per meter. A model injection mechanism is located above the test section and was used to inject the flat-plate model into the test core of the nozzle. A more complete description of the tunnel is given in reference 14.

Model

Figure 1 shows a sketch of the flat-plate model. An existing flat-plate model formerly used in another experiment was modified by installing electrodes for a spark at a location directly in front of one row of thermocouples. Several spark electrode configurations were tested (fig. 2) and all were mounted on a boron nitride insulator. The surface of the boron nitride insulator was flush with the model surface in all tests. The sharp leading edge of the flat plate had a nominal thickness varying from about 0.001 to 0.002 cm. The thermocouple locations shown in figure 1 were design locations; however, many of these thermocouples were lost prior to and during these tests due to model handling so that data are not shown for all locations. As illustrated in figure 1, there is an additional row of thermocouples 5.08 cm to the side of the row which is behind the spark. The thermocouples are spotwelded to the undersurface of detachable plates forming the surface of the flat plate. The stainless-steel plates have a nominal thickness of 0.157 cm; however, the exact thickness at each thermocouple was measured for use in the data reduction. Actual thicknesses were within 0.002 cm of the nominal thickness. The wall-to-free-stream temperature ratio was approximately 5.7 for all tests.

Spark Apparatus

Two types of spark equipment were used for the tests. The major portion of the tests was conducted with a relatively low-power spark, but a limited number of tests used sparking equipment designed to furnish 100 times the power of the low-power spark.

Low-power-spark equipment.- Schematics of the electronic equipment which generated the pulsed-arc voltage during the initial tests are presented in figures 3 and 4. A variable-frequency sine wave from a signal generator drove the NASA designed high-voltage pulse supply. The pulsed high-voltage output, in turn, was connected to the arc electrodes on the model.

The input transistor Q1 is driven into saturation by the positive half of each cycle. The clipped half-wave signal thus obtained drives the power transistor Q2. A 115 volts ac to 6.3 volts ac filament transformer is connected to step up the pulsed collector voltage of Q2 from a peak of 40 volts to approximately 800 volts. The abrupt switching of Q2 into an inductive load results in an approximate square wave across the secondary of the transformer T1.

The circuitry was optimized around an 800-volt pulse level to insure reliability during all tunnel test conditions. The peak power dissipated in the arc was measured at 1.2 watts; at a duty cycle of 0.5 the average power is estimated to be 0.6 watt.

High-power-spark equipment.- For the second series of tests, different equipment provided a higher power input to the spark. Basically, the test apparatus consisted of a

pulse generator and a klystron pulse modulator (fig. 5). The pulse generator was adjusted for a 10-kHz repetition rate, with a pulse width of 100 nsec. This condition results in a 0.001 duty cycle which is the maximum for the pulse modulator unit being used. The output of the pulse generator was connected to the "external trigger" input of the pulse modulator; this provided output pulses to the arc electrodes at the high-voltage supply level. This output was adjustable from 0 to 16 kV. Tests were made with peak power levels measured at 50 kW to 100 kW; the average power is then estimated to be 50 watts and 100 watts, respectively.

Procedures

During both series of tests, procedures were established whereby an operational check of the test apparatus was conducted prior to initiation of tunnel flow. This check was made subsequent to tunnel pump down to verify the establishment of an arc. Visual observation indicated a bright blue glow surrounding the electrodes.

During initiation of tunnel start procedures, the model was in a retracted position and was not visible. After establishment of tunnel flow but before model injection, the arc voltage was applied and the arcing was verified by observing an arc current meter. The model was then injected into the stream.

DATA REDUCTION

The temperature time history of the model surface was recorded during a test by sampling each thermocouple reading 20 times per second. The data thus generated allowed a calculation of the heat transfer to the model at each thermocouple location by equating the aerodynamic heat transfer to the rate of heat storage in the model skin, as follows:

$$\dot{q} = \rho_s c_{p,s} \tau_s \frac{dT}{dt}$$

where for the present tests

$$\rho_s = 8650 \text{ kg/m}^3$$

$$c_{p,s} = 456.5 \text{ joules/kg-K}$$

and τ_s is the measured skin thickness at each thermocouple.

Data sampling began several seconds before the model was injected into an established flow. After the model reached its test position in the stream (approximately 0.3 sec after the start of injection), the heat transfer was computed for each 0.05-sec time interval and then averaged over the first 20 intervals.

The local Stanton number was computed by assuming a laminar recovery factor of 0.845 and a turbulent recovery factor of 0.895. Because the purpose of the investigation was to seek the effect of the spark on transition, an approximate calculation of Stanton number was considered sufficient and any induced pressure effect on the adiabatic wall temperature was neglected.

RESULTS AND DISCUSSION

Schlieren Observations

Schlieren pictures of the flat-plate model in the $M = 8.5$ airstream are shown in figure 6. The pictures were taken with a mercury-arc light source having a nominal light duration of about 8 msec. Figure 6(a) shows the shock pattern with arc off and electrodes against the surface (configuration B) at a unit Reynolds number of 17.5×10^6 per meter. Figures 6(b) and 6(c) show the shock patterns with the low-power spark on the raised electrodes (configuration A) at frequencies of 10 000 and 50 000 Hz, respectively. Figure 6(d) shows the shock pattern with the high-power spark on the rail electrodes (configuration D). There is an elongated spark for this configuration as might be expected. A pair of weak shocks which appear to come from the spark region in figures 6(b) and 6(c) are present just as strongly in figure 6(a); therefore, these shocks must be associated with the electrodes or plate surface discontinuities.

Heat-Transfer Data

The Stanton number was obtained from heating-rate data and is plotted against the local Reynolds number of each thermocouple location. Figure 7 gives typical results and shows a comparison of the heat-transfer data for the three electrode configurations used with the low-power spark. All data compared in figure 7 are with the spark inoperative. The dash-line curve in the lower Reynolds number range is the theoretical laminar-heat-transfer prediction using the Monaghan T' method (ref. 15) and the dash-line curve in the upper Reynolds number range is the turbulent-heat-transfer prediction using the modified Spalding-Chi method (refs. 16 and 17) and assuming that the virtual origin is taken at the location of peak heating from the configuration A data. These data (fig. 7) indicate a forward movement of both the start of transition and the end of transition for the raised-electrode configuration (configuration A, fig. 2) as compared with data for row B and the other types of electrodes. This forward movement is believed to be due to the roughness effect of the raised electrodes. The local Reynolds number corresponding to the electrode location is 0.40×10^6 for these tests at a unit Reynolds number of 11.6×10^6 per meter and the boundary-layer thickness at the electrode location is estimated to be about 0.11 cm. Thus, the raised-electrode configuration concentrates its major disturbance at a point about 0.7 of the boundary-layer thickness from the wall. The forward movement

of transition due to the roughness effect from the raised electrodes is significant but it is still far downstream of the electrode location. The roughness effect of the raised-electrode configuration also produces an increase in the laminar heating ahead of transition. Within the data scatter, there appears to be no roughness effect for the two other configurations.

Figure 8 shows the effect of the 10-kHz low-power spark for each electrode configuration. Although for the raised-electrode configuration the end of transition appears to move slightly, the data show essentially no movement of the beginning of transition due to the presence of the spark (figs. 7 and 8(a)). Figure 8(a) also shows that the spark produces an additional increase in the heating on the laminar region above that which occurs for the raised-electrode configuration with the spark inoperative. For configurations B and C, the spark has no observable effect on the beginning of transition and the end of transition occurs beyond the data sample.

Effect of spark frequency.- In selecting the spark-frequency range for experimental investigation, a useful guideline is the stability theory of Mack (ref. 18). Although there is no proof of an accurate relationship between the predictions of stability theory and the start of transition, the theory is used here in a qualitative manner only to identify the range of frequencies to which the boundary layer might be most sensitive. Figure 9 shows a neutral stability diagram taken from reference 18. On a plot of wave number as a function of the square root of Reynolds number the boundaries for both $M = 7$ and $M = 10$ flow are shown. The local Mach number for the present tests is lower than the free-stream value of 8.5 due to induced pressure effects and therefore the Mach 7 boundary in figure 9 is the more applicable. Small periodic perturbations inside the neutral stability boundaries should tend to be unstable and would be amplified, whereas outside the boundaries such perturbations should be damped. The vertical arrows at a value of $\sqrt{N_{Re,x}} = 1414$ show the relationship between the spark frequencies for the tunnel conditions of the present tests and the stability boundaries. A Reynolds number value of 2×10^6 was selected since this is about the maximum extent of laminar flow for the present tests at both the high and low test values of unit Reynolds number. The calculated boundary-layer thickness δ on the flat-plate model at a Reynolds number of 2×10^6 enters into the determination of wave number and the value of δ was determined from the T' method of Monaghan using temperature-velocity relationships of Crocco as given in reference 19.

The results shown in figure 9 indicate that the tests with a 10-kHz spark frequency are in a range where amplification of periodic disturbances should occur. Conversely, the tests with a spark frequency of 50 kHz are well above the predicted neutral stability boundary.

The free-stream velocity in the wind tunnel was 1254 m/sec. At a location of 0.7 of the boundary-layer thickness from the wall, the velocity is approximately 85 percent of free-stream velocity. Thus, if 10 000 sparks/sec were generated at this location, the distance between disturbances if they moved with the local flow velocity would be about 10 cm. At a frequency of 50 kHz, the distance between disturbances would be about 2 cm. These numbers are quoted to illustrate the physical picture occurring with the multiple sparks on the plate and to illustrate that with too low a frequency the distance between sparks could easily be too great to produce a cumulative effect of multiple sparks.

Data were taken for spark frequencies of 10 kHz and 50 kHz with the low-power spark and these results are compared with the data for the spark inoperative in figure 10. Figure 10(a) shows the raised-electrode configuration at a unit Reynolds number of 11.6×10^6 per meter. No forward movement of the start of transition is apparent and increasing the frequency from 10 kHz to 50 kHz apparently lowers the laminar heating to a value comparable to that with the spark inoperative. The data show the end of transition to agree with spark inoperative data. The data of figure 10 show evidence of more sensitivity of the laminar boundary layer to a 10-kHz frequency disturbance than to a 50-kHz frequency disturbance as predicted by the neutral stability boundary of figure 9; however, the evidence is not overwhelming.

Although data were taken for only two frequencies, the spark frequency was gradually changed in some tests while visually monitoring the thermocouple output. This slow scan of frequencies for configuration A during a test failed to detect any critical frequency in the range from 10 kHz to 50 kHz. Visual monitoring of thermocouple outputs, however, is not the most sensitive indicator of small changes; thus, the results of this slow scan should not be considered conclusive. A fast-response steady-state type of heat gage, which indicates heat transfer directly, would be more appropriate for any visual monitoring of the change in heating rate with frequency. Figure 10(b) shows data for a higher unit Reynolds number than that of figure 10(a) and the general level of laminar heating is seen to increase. Also, some tendency for the 10-kHz spark to produce higher laminar heating than the 50-kHz spark is evident. However, the spark apparently has no usefulness in producing any change in transition location for these test conditions.

High-power-spark results.- Test results obtained with the high-power supply (fig. 5) are shown in figure 11. For this series of tests, the rail electrodes (configuration D) were used. Results obtained with no spark, a 50-watt spark, and a 100-watt spark are compared in figure 11. There is no significant effect of this spark on transition. The increase in laminar heating is probably due to the roughness effect of the electrodes, which, in view of the extremely high heating levels, could be dominating the transition process and overshadowing any effect of the spark. The flagged symbols show Stanton number values for thermocouple row B which is located 5.08 cm laterally from row A (fig. 1) and these data indicate a normal level of laminar heating.

CONCLUDING REMARKS

The results of an experimental investigation into the use of a high-frequency spark to induce early transition on a flat-plate model at Mach number 8.5 were essentially negative. Four electrode configurations, a frequency range from 10 kHz to 50 kHz, and various power inputs to the spark were investigated. For the raised-electrode configuration (0.051-cm-diameter wire bent horizontal to the plate in the lateral direction at 0.076 cm above the plate), the electrode served as a roughness element and produced some forward movement of transition and raised the laminar heating in the region behind the electrode when the spark was inoperative. No significant forward movement of the beginning of transition occurred due to the spark for any of the electrode configurations as compared with the beginning of transition with the spark inoperative. Stability theory predicts that for the conditions of the present tests, the laminar boundary layer should be more unstable to the 10-kHz spark than to the 50-kHz spark, and the data indicate a slight tendency for the laminar heating to be higher for the 10-kHz spark than for the 50-kHz spark. However, there was essentially no change in transition location with frequency.

Langley Research Center,
National Aeronautics and Space Administration,
Hampton, Va., July 17, 1972.

REFERENCES

1. Morrisette, E. Leon; Stone, David R.; and Whitehead, Allen H., Jr.: Boundary-Layer Tripping With Emphasis on Hypersonic Flows. Viscous Drag Reduction, C. Sinclair Wells, ed., Plenum Press, 1969, pp. 33-51.

2. Holloway, Paul F.; and Sterrett, James R.: Effect of Controlled Surface Roughness on Boundary-Layer Transition and Heat Transfer at Mach Numbers of 4.8 and 6.0. NASA TN D-2054, 1964.

3. Sterrett, James R.; Morrisette, E. Leon; Whitehead, Allen H., Jr.; and Hicks, Raymond M.: Transition Fixing for Hypersonic Flow. NASA TN D-4129, 1967.

4. Potter, J. Leith; and Whitfield, Jack D.: Effects of Unit Reynolds Number, Nose Bluntness, and Roughness on Boundary Layer Transition. AEDC-TR-60-5, U.S. Air Force, Mar. 1960.

5. Whitehead, Allen H., Jr.: Flow-Field and Drag Characteristics of Several Boundary-Layer Tripping Elements in Hypersonic Flow. NASA TN D-5454, 1969.

6. Fage, A.; and Sargent, R. F.: An Air-Injection Method of Fixing Transition From Laminar to Turbulent Flow in a Boundary Layer. R. & M. No. 2106, Brit. A.R.C., 1944.

7. Coles, Donald: Measurements in the Boundary Layer on a Smooth Flat Plate in Supersonic Flow – III. Measurements in a Flat-Plate Boundary Layer at the Jet Propulsion Laboratory. Rep. No. 20-71 (Contract No. DA-04-495-Ord 18), Jet Propulsion Lab., California Inst. Technol., June 1, 1953.

8. Korkegi, Robert H.: Transition Studies and Skin-Friction Measurements on an Insulated Flat Plate at a Mach Number of 5.8. J. Aeronaut. Sci., vol. 23, no. 2, Feb. 1956, pp. 97-107, 192.

9. Stone, David Ray: The Effect of Discrete Jets Used as a Boundary Layer Trip on Transition, Heat Transfer, and the Downstream Flowfield at Mach Numbers of 6.0 and 8.5. M.S. Thesis, North Carolina State Univ., 1971.

10. Deimen, James M.; and Clark, John A.: An Experimental Study of the Influence of Localized, Normal Surface Oscillations on the Laminar Flow Over a Flat Plate. ARL-66-0010, Pt. VI, U.S. Air Force, Jan. 1966. (Available from DDC as AD 639 444.)

11. Jackson, Francis J.; and Heckl, Manfred A.: Effect of Localized Acoustic Excitation on the Stability of a Laminar Boundary Layer. ARL 62-362, U.S. Air Force, June 1962.

12. Velkoff, Henry R.; and Ketcham, Jeffry: Effect of an Electrostatic Field on Boundary-Layer Transition. AIAA J., vol. 6, no. 7, July 1968, pp. 1381-1383.

13. Klein, Enrique J.: Excitation of Boundary-Layer Turbulence Through Spark Discharges. NASA TN D-6378, 1971.

14. Schaefer, William T., Jr.: Characteristics of Major Active Wind Tunnels at the Langley Research Center. NASA TM X-1130, 1965.

15. Monaghan, R. J.: An Approximate Solution of the Compressible Laminar Boundary Layer on a Flat Plate. R. & M. No. 2760, Brit. A.R.C., 1953.

16. Spalding, D. B.; and Chi, S. W.: The Drag of a Compressible Turbulent Boundary Layer on a Smooth Flat Plate With and Without Heat Transfer. J. Fluid Mech., vol. 18, pt. 1, Jan. 1964, pp. 117-143.

17. Bertram, Mitchel H.; and Neal, Luther, Jr.: Recent Experiments in Hypersonic Turbulent Boundary Layers. Presented at the AGARD Specialists Meeting on Recent Developments in Boundary-Layer Research (Naples, Italy), May 1965. (Also available as NASA TM X-56335.)

18. Mack, Leslie M.: Boundary-Layer Stability Theory. 900-277 Rev. A (Contract No. NAS 7-100), Jet Propulsion Lab., California Inst. Technol., Nov. 1969.

19. Van Driest, E. R.: Investigation of Laminar Boundary Layer in Compressible Fluids Using the Crocco Method. NACA TN 2597, 1952.

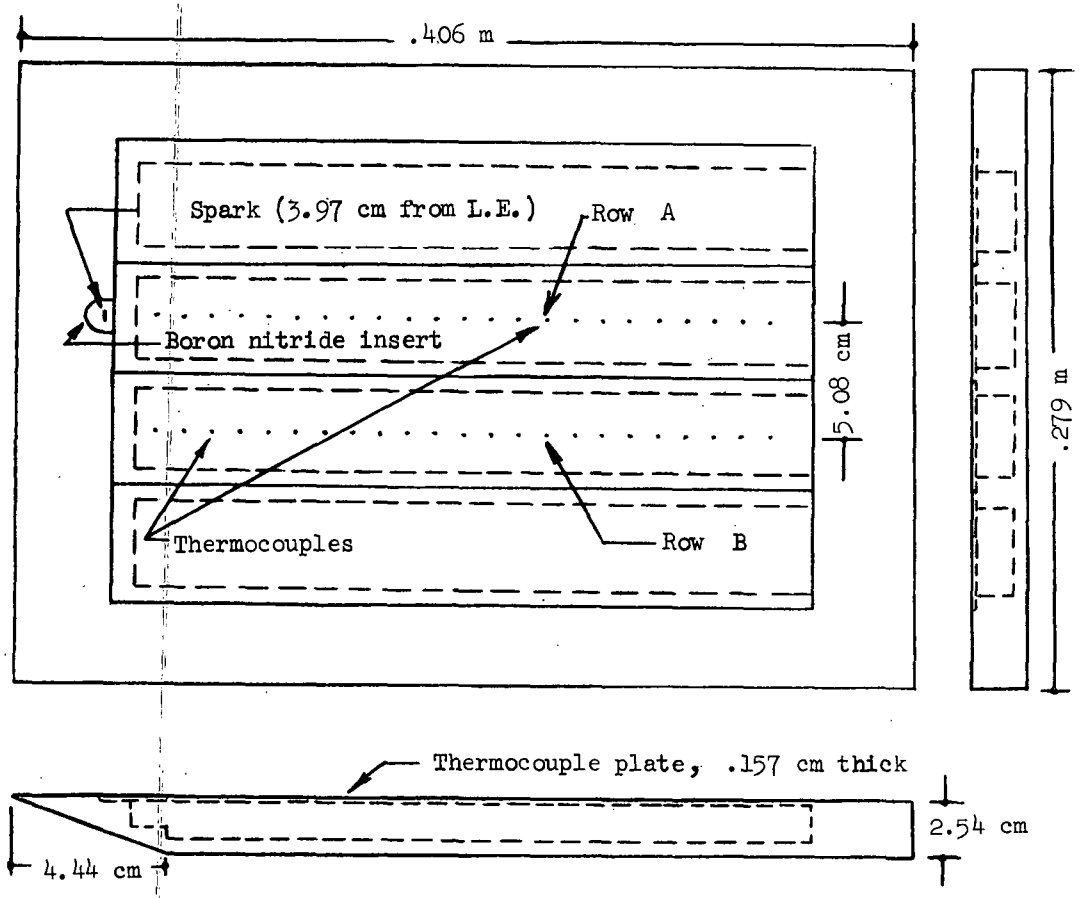

Thermocouple locations

(Rows A and B have identical distances from L.E.)

Thermocouple	Centimeters
1	6.35
2	7.62
3	8.89
4	10.16
5	11.43
6	12.70
7	13.97
8	15.24
9	16.51
10	17.78
11	19.05
12	20.32
13	21.59
14	22.86
15	24.13
16	25.40
17	26.67
18	27.94
19	29.21
20	30.48
21	31.75
22	33.02
23	34.29

Figure 1.- Sketch of flat-plate model.

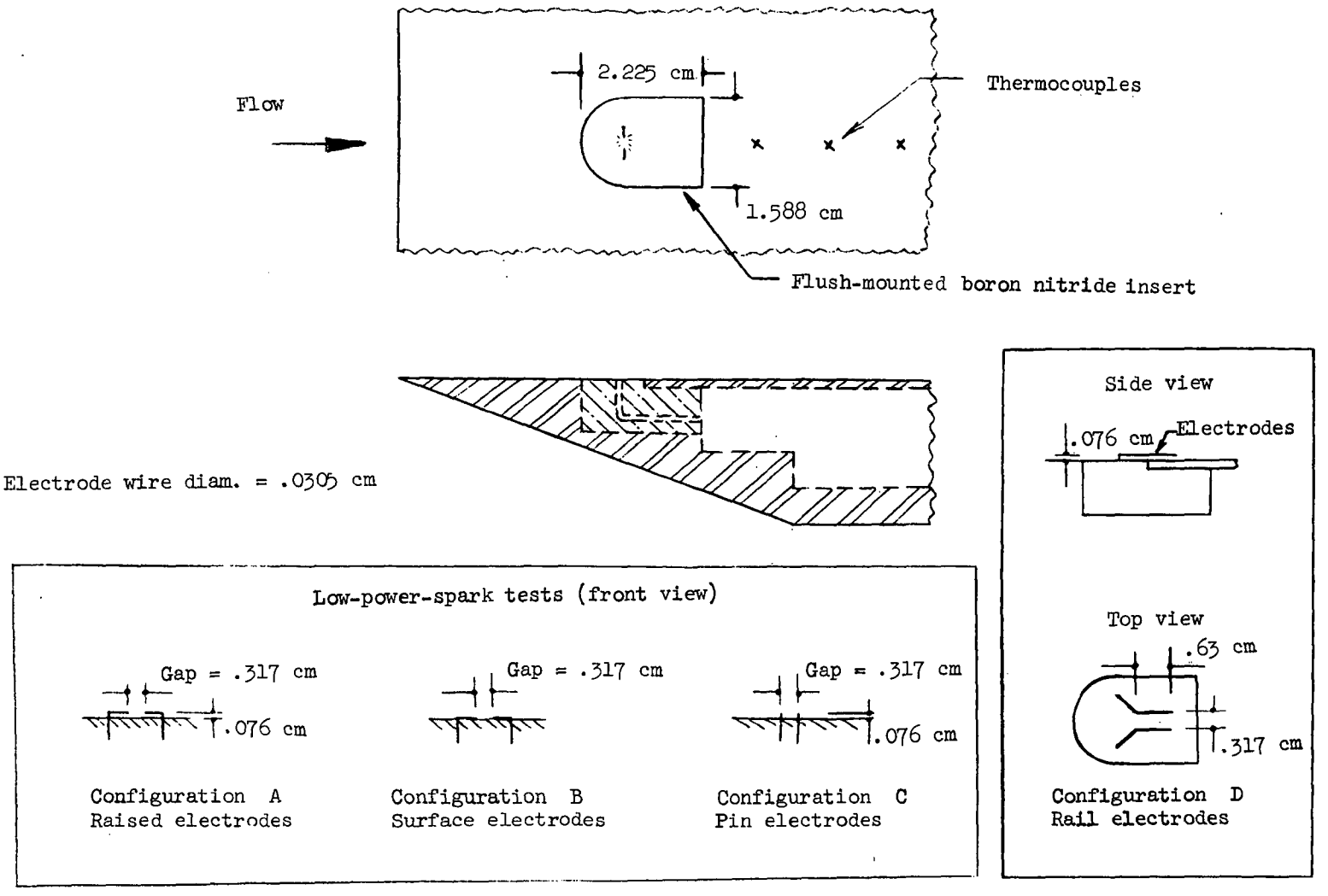

Figure 2.- Sketches of electrode configurations.

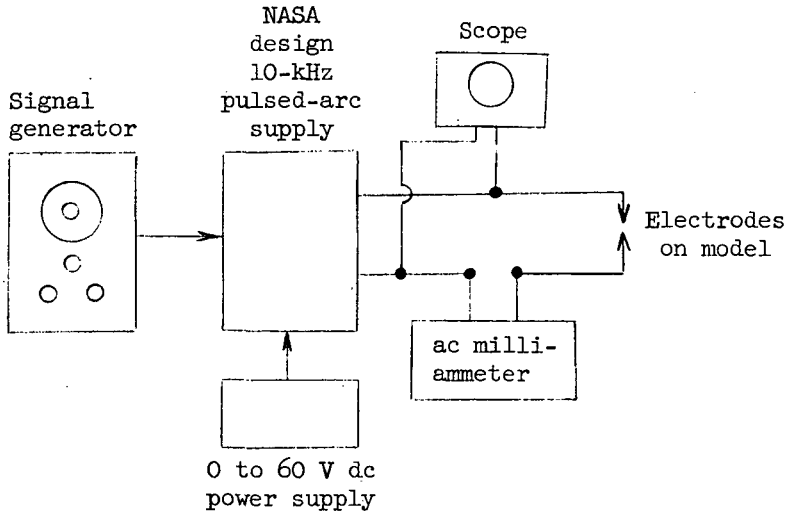

Figure 3.- Block diagram of test apparatus for low-power-spark tests.

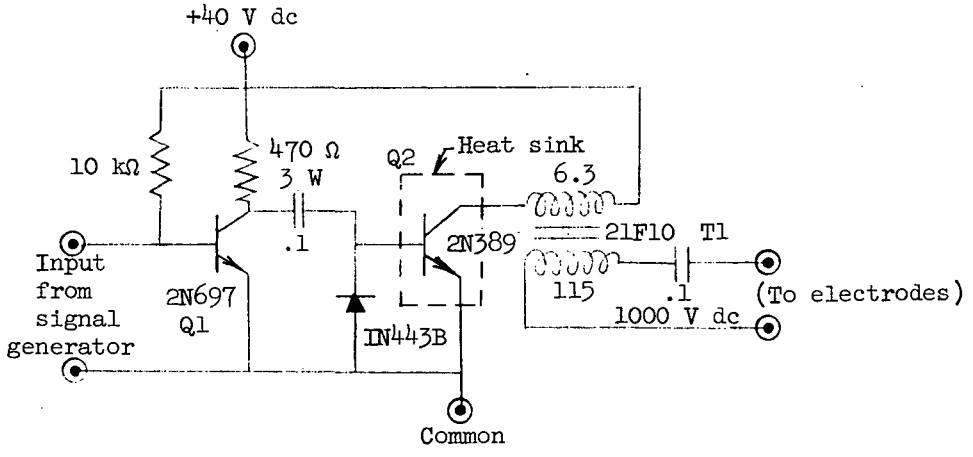

Figure 4.- Schematic of 10 kHz pulsed-arc supply for low-power-spark tests.

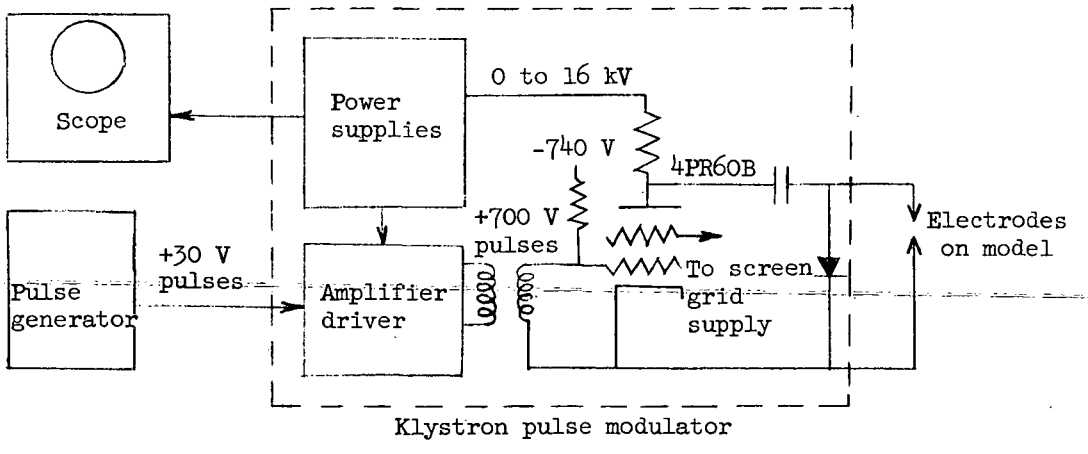

Figure 5.- Block-diagram/schematic of test apparatus for high-power-spark tests.

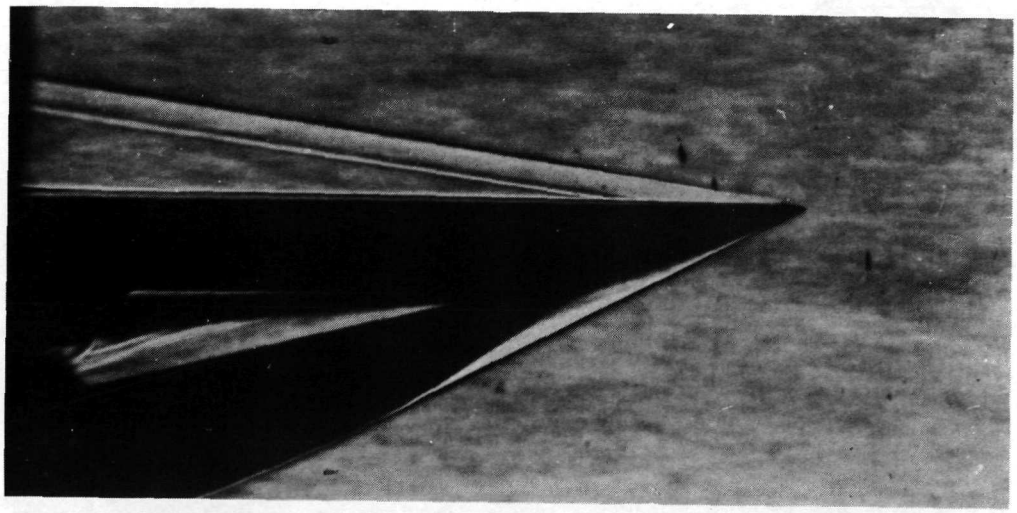

(a) No spark; electrodes on surface; configuration B.

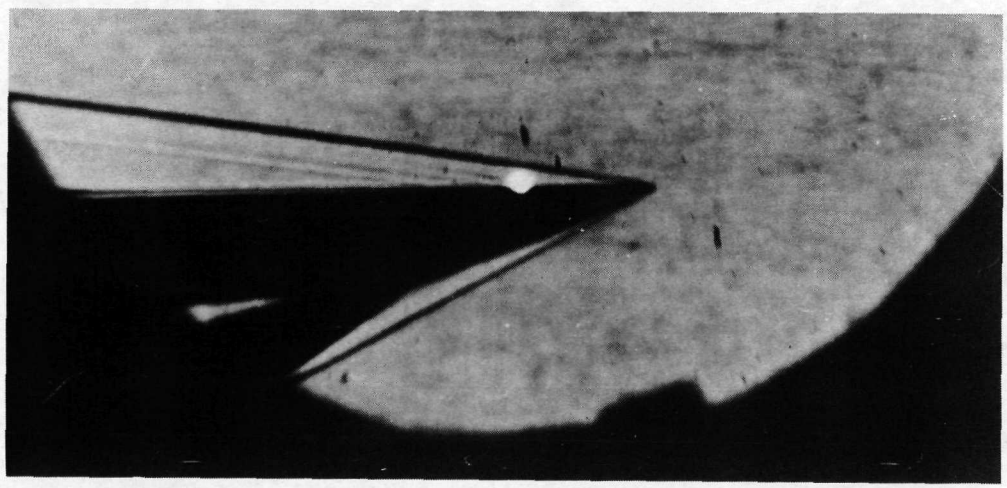

L-72-2473

(b) Frequency, 10 000 Hz; raised electrodes; configuration A.

Figure 6.- Schlieren photographs of flow. $N_{Re} = 17.5 \times 10^6$ per meter.

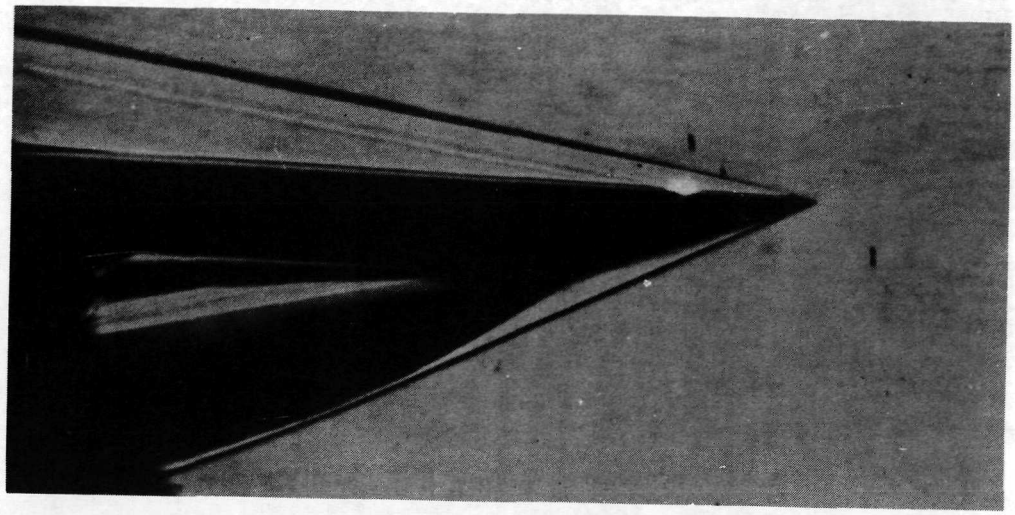

(c) Frequency, 50 000 Hz; raised electrodes; configuration A.

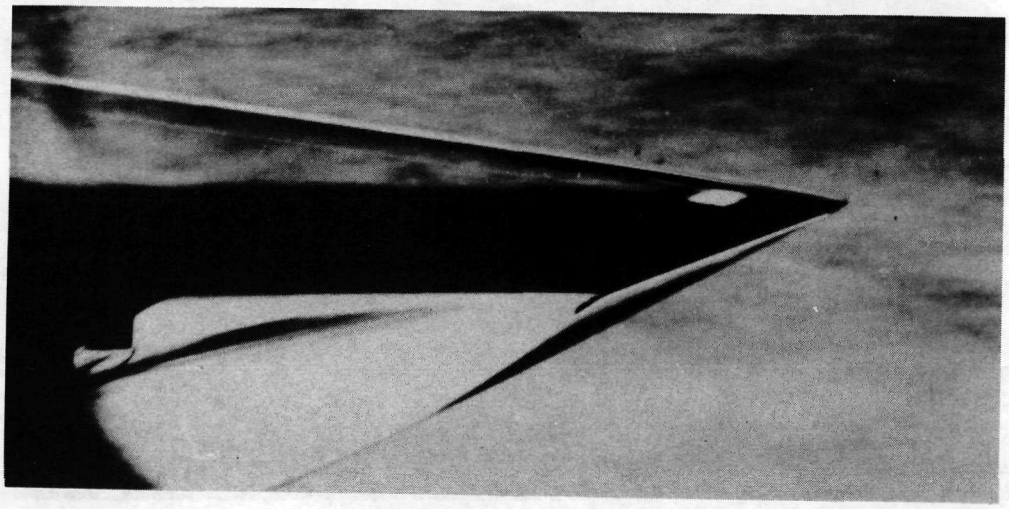

L-72-2474

(d) Frequency, 10 000 Hz; rail electrodes; configuration D.

Figure 6.- Concluded.

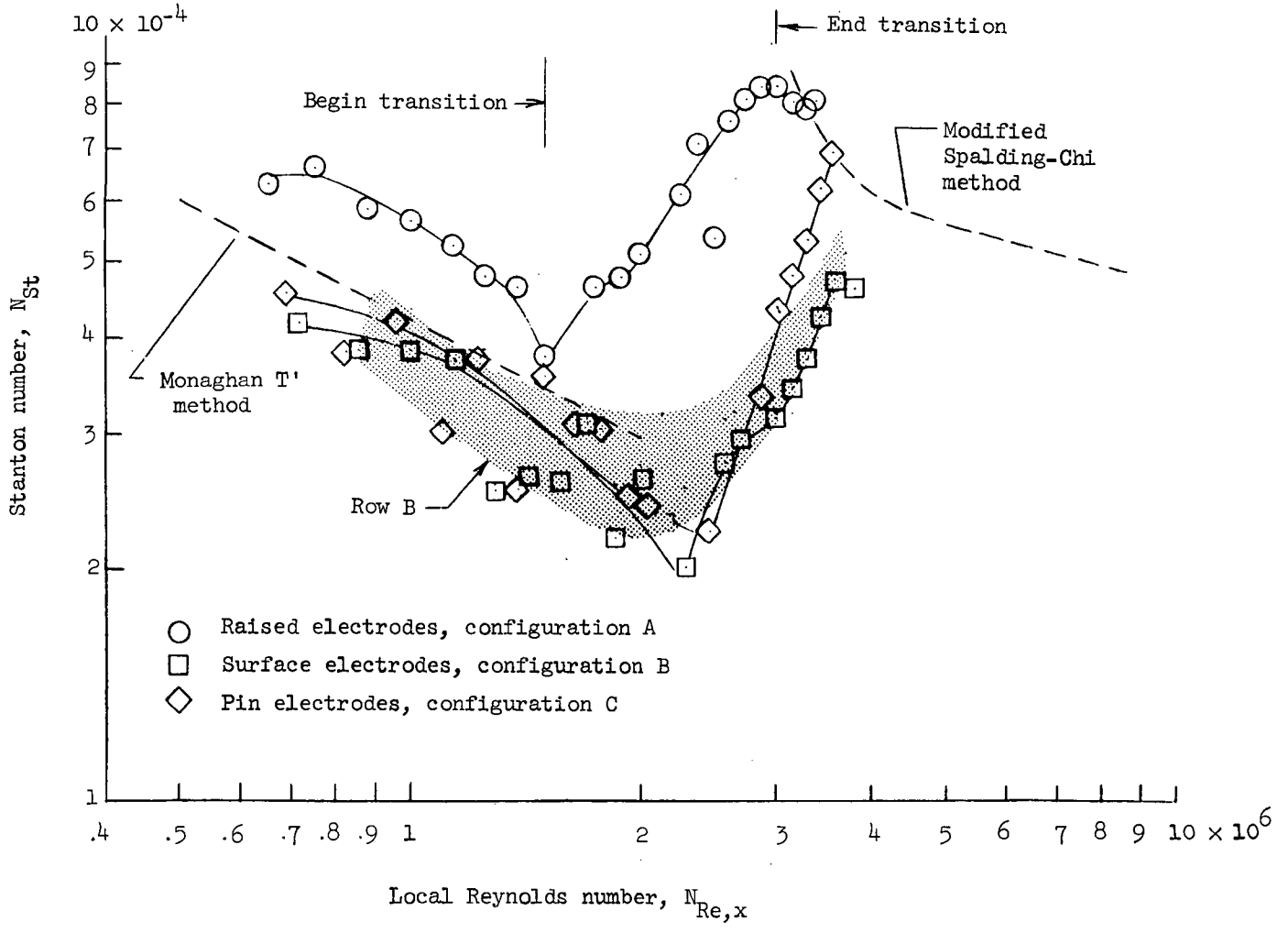

Figure 7.- Effect of electrode configuration. Spark inoperative; $N_{Re} = 11.6 \times 10^6$ per meter.

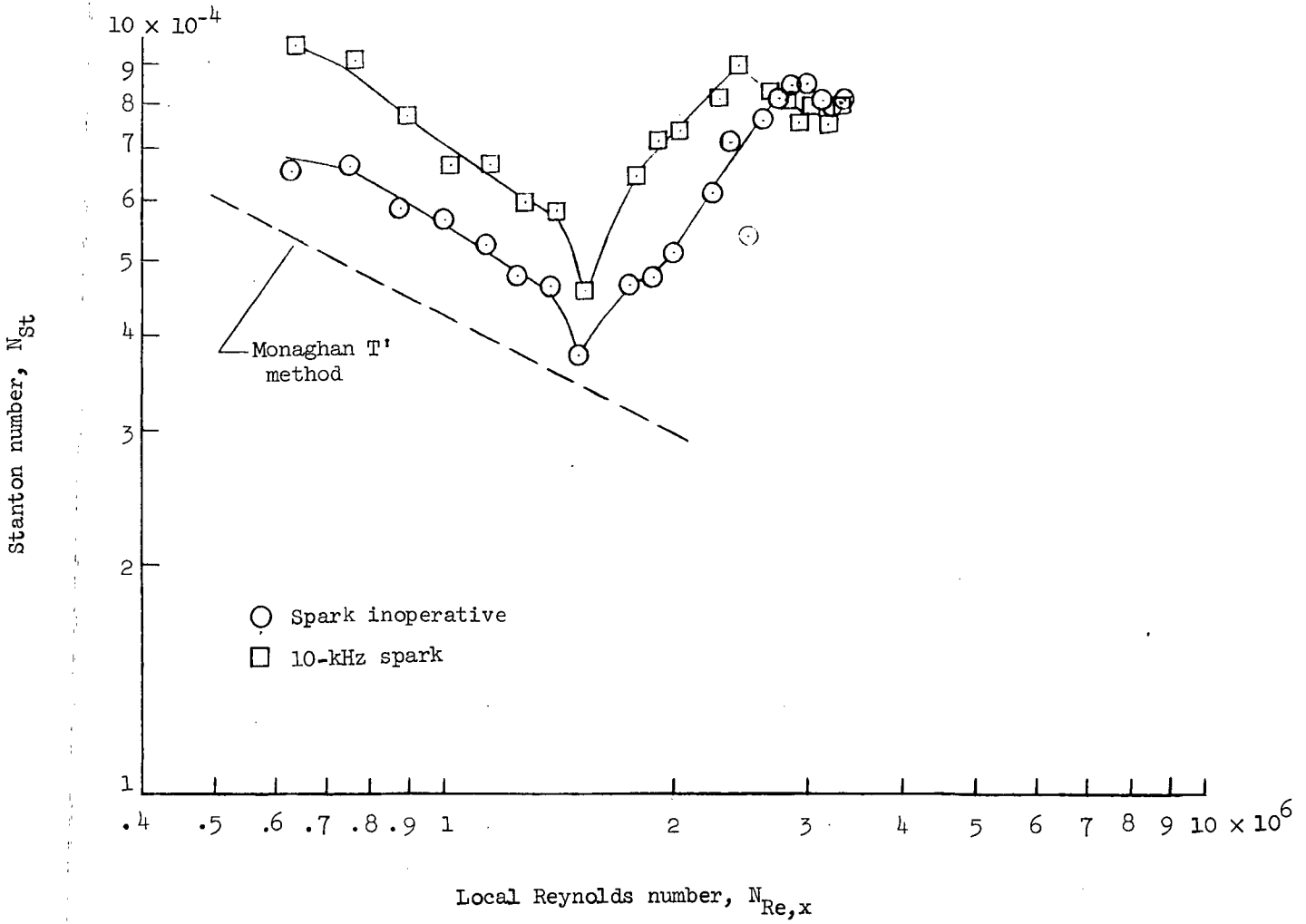

(a) Raised electrodes (configuration A).

Figure 8.- Effect of 10-kHz spark. $N_{Re} = 11.6 \times 10^6$ per meter.

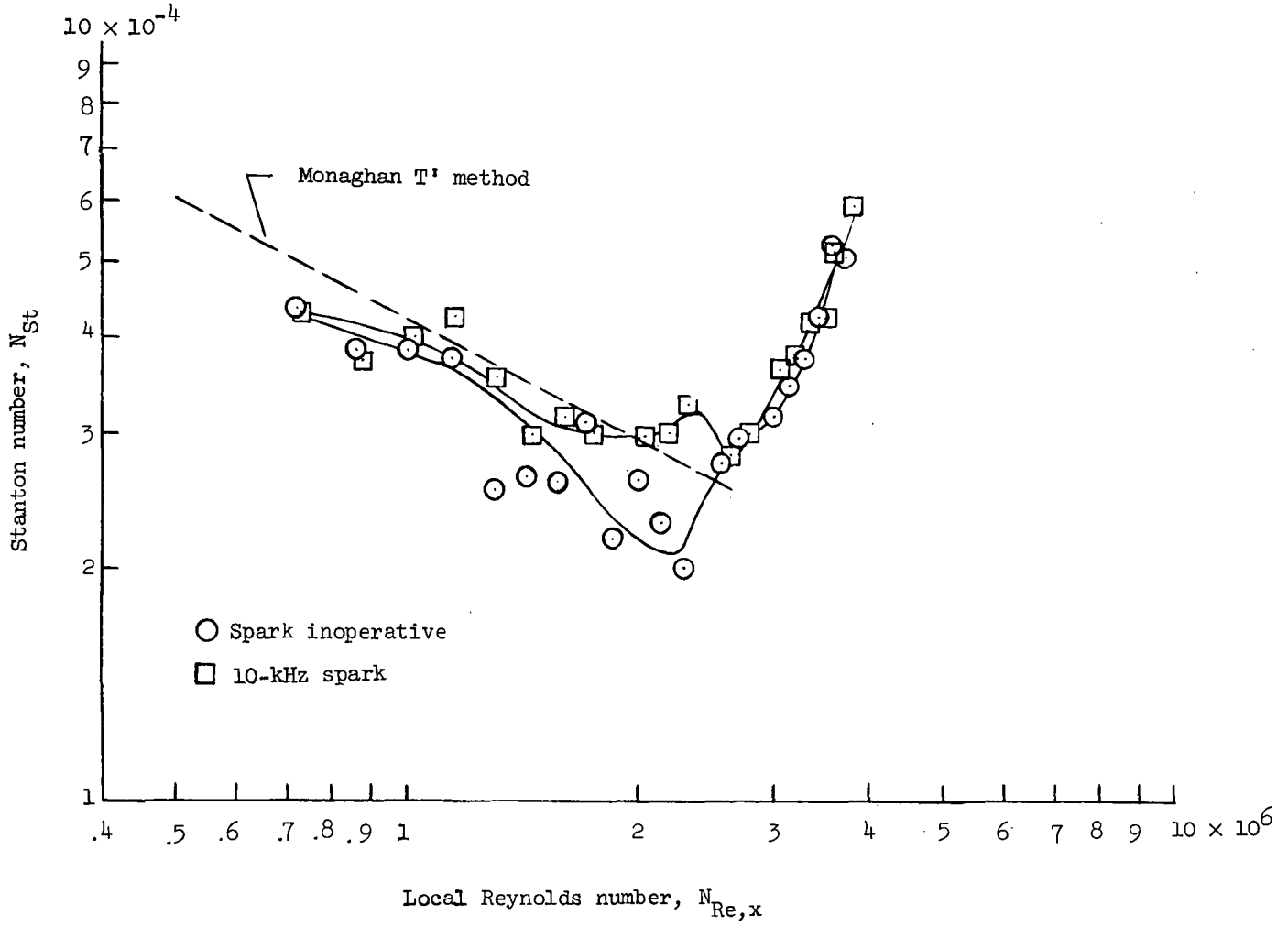

(b) Surface electrodes (configuration B).

Figure 8.- Continued.

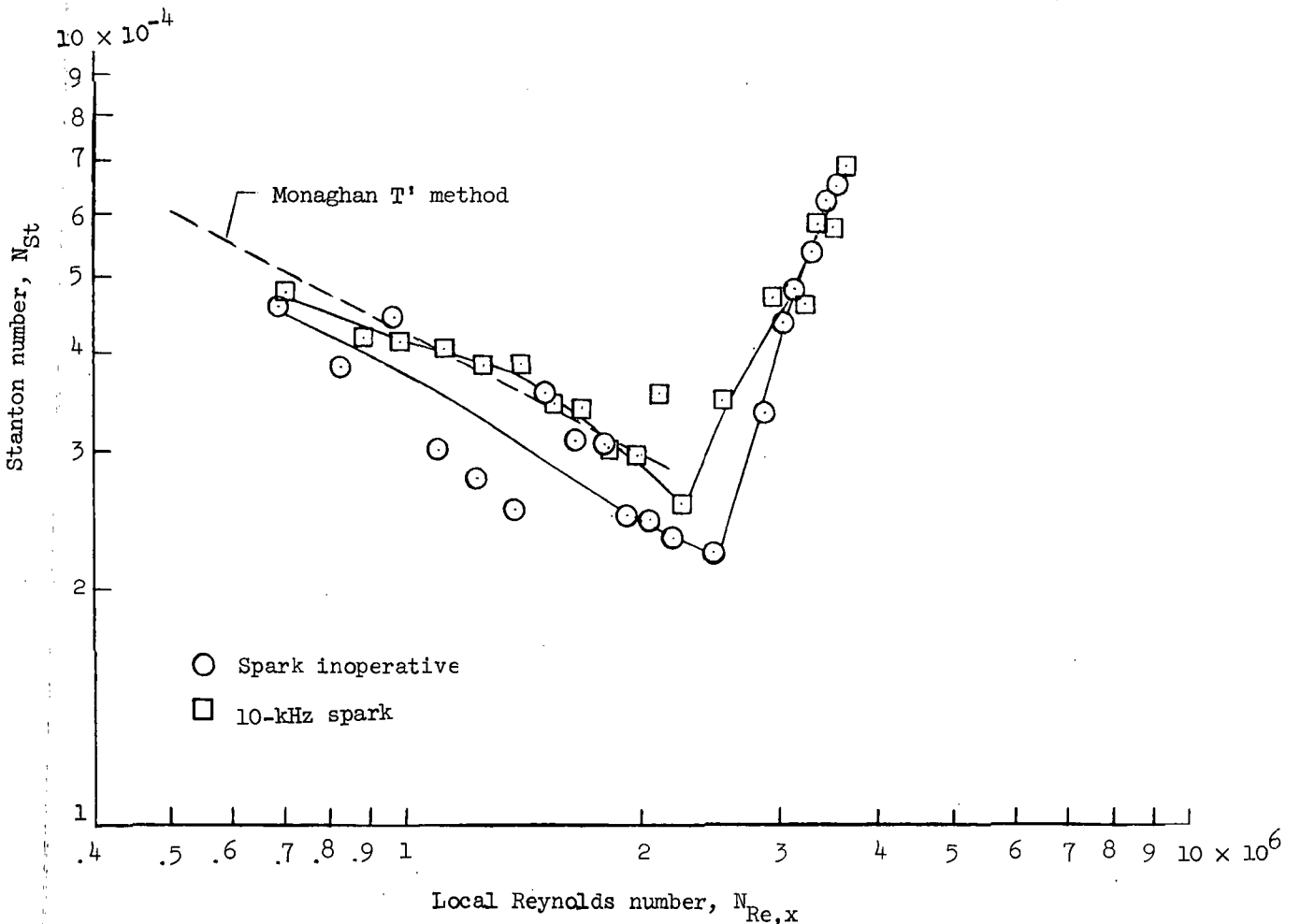

(c) Pin electrodes (configuration C).

Figure 8.- Concluded.

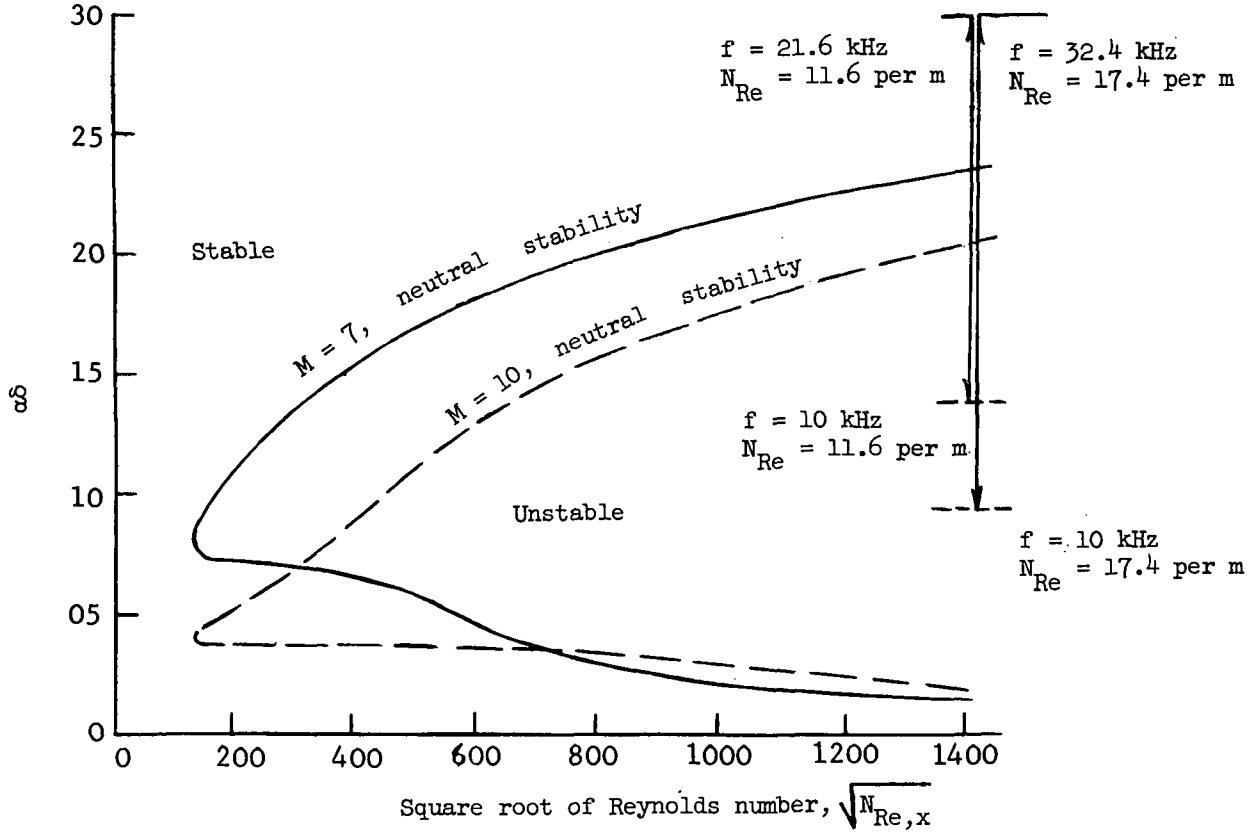

Figure 9.- Test frequency range and theoretical neutral stability curves of reference 18.

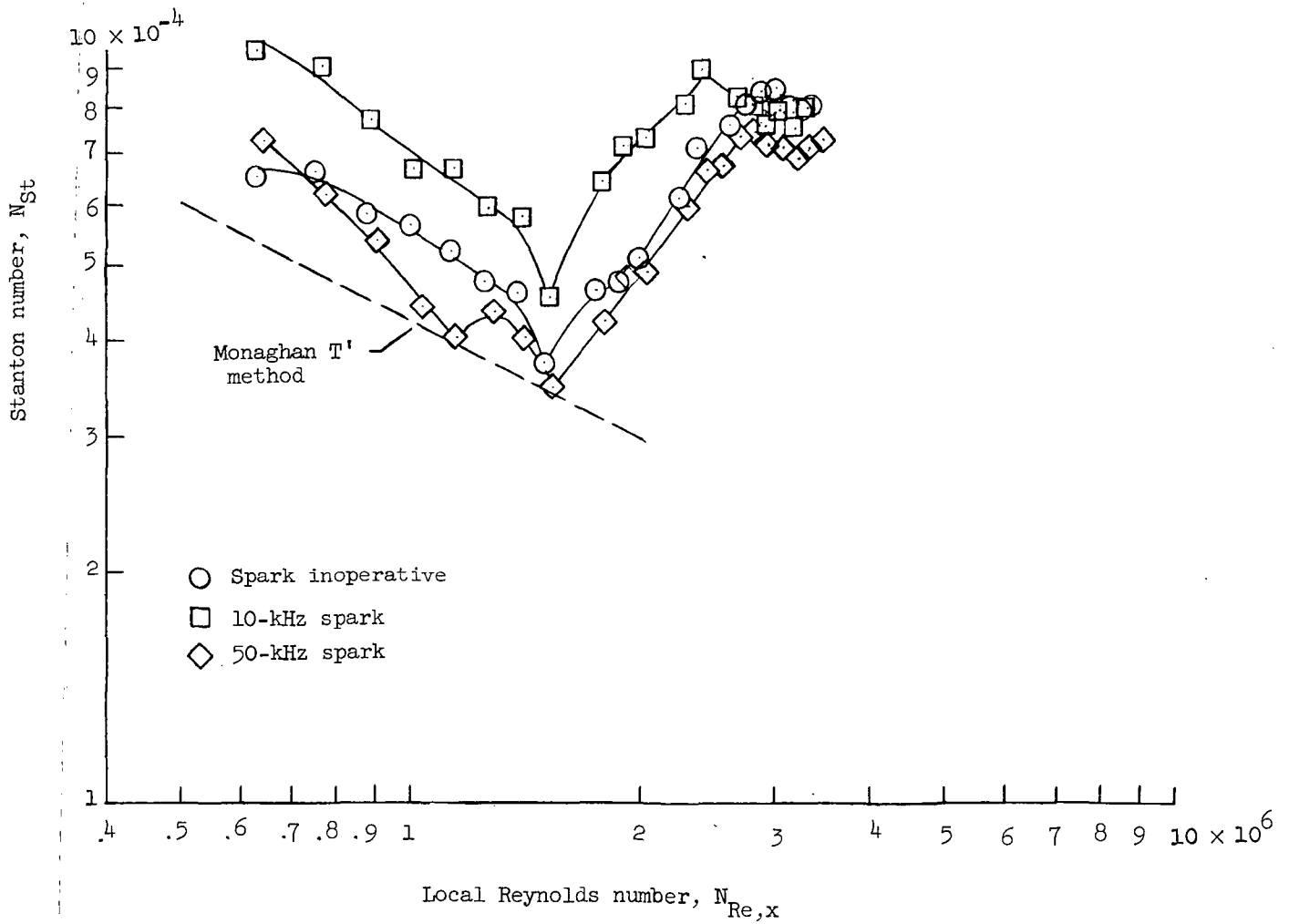

(a) $N_{Re} = 11.6 \times 10^6$ per meter.

Figure 10.- Effect of spark frequency. Raised electrodes (configuration A).

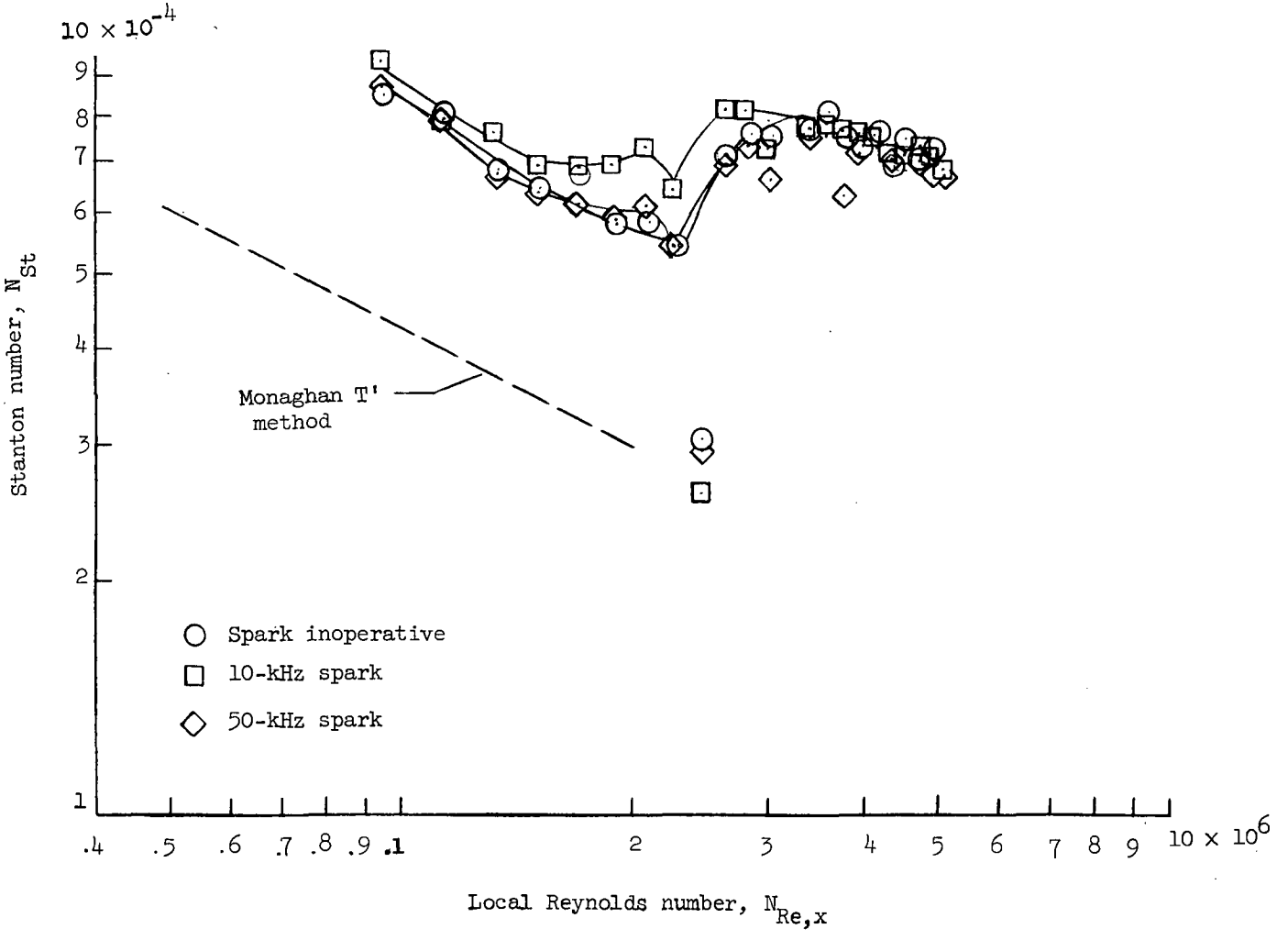

(b) $N_{Re} = 17.4 \times 10^6$ per meter.

Figure 10.- Concluded.

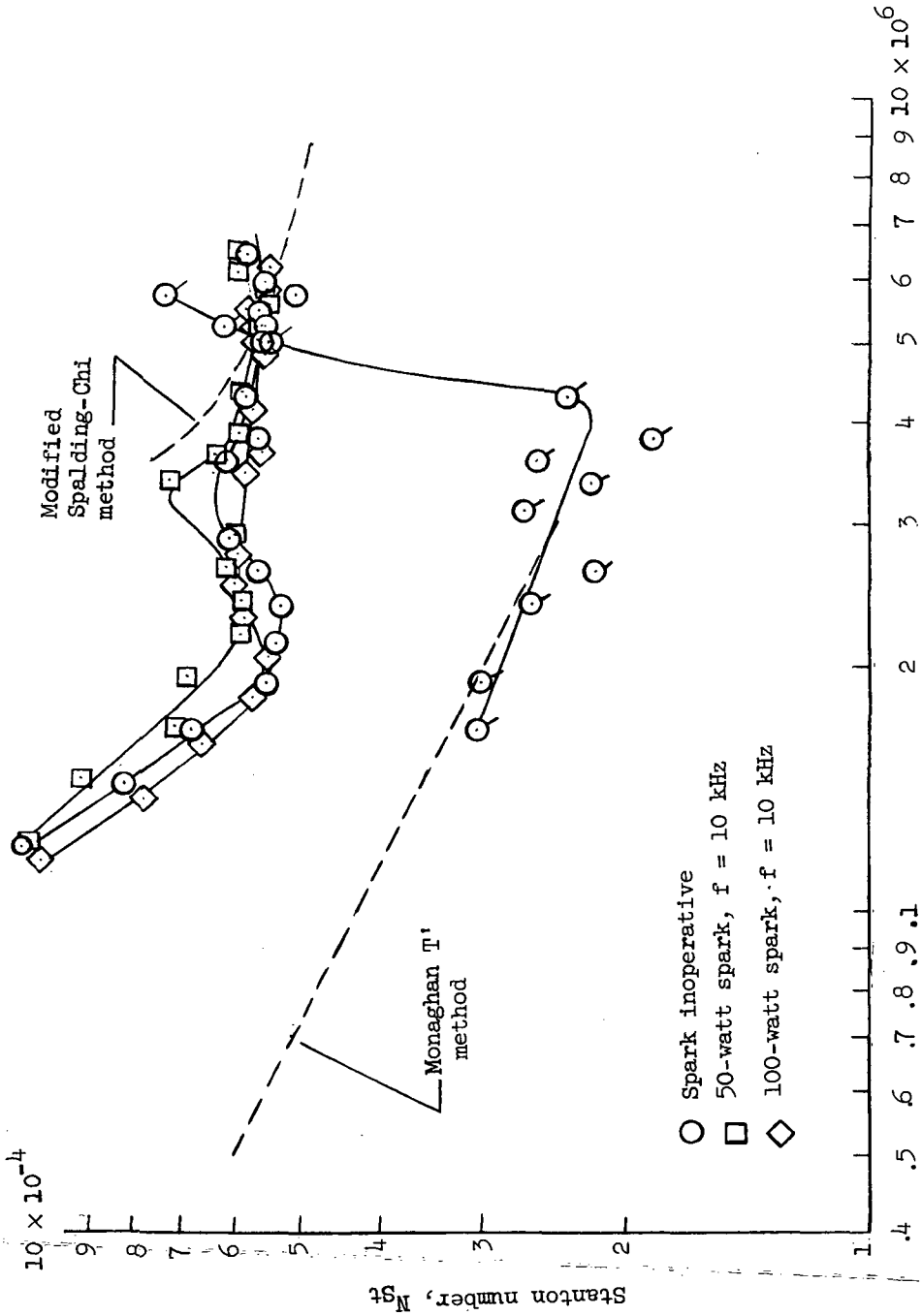

Figure 11.- Effect of spark power level. Rail electrodes (configuration D); $N_{Re} = 18.6 \times 10^6$ per meter. Flagged symbols denote data from thermocouple row B.

NASA-Langley, 1972 —— 12 L-8314

NATIONAL AERONAUTICS AND SPACE ADMISTRATION
WASHINGTON D.C. 20546

OFFICIAL BUSINESS
PENALTY FOR PRIVATE USE $300

FIRST CLASS MAIL

POSTAGE AND FEES PAID
NATIONAL AERONAUTICS AND
SPACE ADMINISTRATION

U.S.MAIL

NASA 451

POSTMASTER: If Undeliverable (Section 158 Postal Manual) Do Not Return

"The aeronautical and space activities of the United States shall be conducted so as to contribute . . . to the expansion of human knowledge of phenomena in the atmosphere and space. The Administration shall provide for the widest practicable and appropriate dissemination of information concerning its activities and the results thereof."

—NATIONAL AERONAUTICS AND SPACE ACT OF 1958

NASA SCIENTIFIC AND TECHNICAL PUBLICATIONS

TECHNICAL REPORTS: Scientific and technical information considered important, complete, and a lasting contribution to existing knowledge.

TECHNICAL NOTES: Information less broad in scope but nevertheless of importance as a contribution to existing knowledge.

TECHNICAL MEMORANDUMS: Information receiving limited distribution because of preliminary data, security classification, or other reasons.

CONTRACTOR REPORTS: Scientific and technical information generated under a NASA contract or grant and considered an important contribution to existing knowledge.

TECHNICAL TRANSLATIONS: Information published in a foreign language considered to merit NASA distribution in English.

SPECIAL PUBLICATIONS: Information derived from or of value to NASA activities. Publications include conference proceedings, monographs, data compilations, handbooks, sourcebooks, and special bibliographies.

TECHNOLOGY UTILIZATION PUBLICATIONS: Information on technology used by NASA that may be of particular interest in commercial and other non-aerospace applications. Publications include Tech Briefs, Technology Utilization Reports and Technology Surveys.

Details on the availability of these publications may be obtained from:

SCIENTIFIC AND TECHNICAL INFORMATION OFFICE

NATIONAL AERONAUTICS AND SPACE ADMINISTRATION

Washington, D.C. 20546